Revisiting the Equatorial Pacific Sea Surface Temperature Response to Global Warming

Qiuxian Li (liqiuxiande@163.com)
Ocean University of China https://orcid.org/0000-0002-7246-5910
Yiyong Luo
Ocean University of China
Jian Lu
Pacific Northwest National Laboratory
Fukai Liu
Ocean University of China

Research Article

Keywords: Pacific Ocean, Tropics, Sea surface temperature, Climate change, Ocean dynamics

Posted Date: August 31st, 2023

DOI: https://doi.org/10.21203/rs.3.rs-3256971/v1

Version of Record: A version of this preprint was published at Climate Dynamics on December 2nd, 2023. See the published version at https://doi.org/10.1007/s00382-023-07019-8.

Revisiting the Equatorial Pacific Sea Surface Temperature Response to Global Warming

Qiuxian Li[1,2], Yiyong Luo[1,2*], Jian Lu[3], and Fukai Liu[1,2]

[1] *Frontier Science Center for Deep Ocean Multispheres and Earth System (FDOMES) and Physical Oceanography Laboratory, Ocean University of China, Qingdao, China.*

[2] *College of Oceanic and Atmospheric Sciences, Ocean University of China, Qingdao, China.*

[3] *Atmospheric Sciences and Global Change Division, Pacific Northwest National Laboratory, Richland, WA, USA*

Corresponding author: Yiyong Luo (yiyongluo@ouc.edu.cn)

ABSTRACT

The relative roles of the oceanic and atmospheric processes in the pattern formation of the equatorial Pacific sea surface temperature (SST) response to global warming is investigated using a set of climate model experiments embedded with a novel partial coupling technique. The modeling results show that the SST response experiences a transition from a La Niña-like warming pattern at the initial stage to an El Niño-like warming pattern at the quasi-equilibrium stage. By decomposing anomalous equatorial Pacific SST into atmosphere-forced *passive* component and ocean dynamically induced *active* component, it is found that the SST warming pattern at both stages is entirely induced by its *active* component. Specifically, the meridional and vertical ocean circulation changes play a dominant role in forming the La Niña-like SST warming pattern at the initial stage, and the zonal and meridional ocean circulation changes are responsible for the formation of the El Niño-like SST warming pattern at the quasi-equilibrium stage. In contrast, the *passive* SST at both stages is characterized by a zonally uniform warming along the equator, which can be explained by a balance between the total effect of the heat transport divergence associated with the mean ocean circulation and the effect of the *passive* surface heat flux change. In addition, this study finds that it is the slowdown of the Pacific subtropical cells during the transition period that controls the evolution of the equatorial SST warming pattern by changing the meridional and vertical ocean heat transports.

Keywords: Pacific Ocean; Tropics; Sea surface temperature; Climate change; Ocean dynamics

1 Introduction

Given its active air-sea dynamic coupling and profound impact on a variety of climate phenomena such as tropical cyclone activity and ENSO variability (Jin 1996; Fedorov and Philander 2000; Schneider et al. 2009; Collins et al. 2010; DiNezio et al. 2012; Hu and Fedorov 2017), considerable effort has been made to understand how the tropical Pacific sea surface temperature (SST) may change in response to global warming (Clement et al. 1996; Collins 2005; Liu et al., 2005; Xie et al. 2010; Lu and Zhao 2012; Ma and Yu 2014; Luo et al. 2015; Luo et al. 2017; Heede et al. 2020, 2021; Seager et al. 2022; Ying et al. 2022). Typical features of the tropical Pacific SST warming pattern have been identified and studied in previous literature. For example, modelling studies have found a robust equatorially peaked warming pattern, which is attributed to climatological minimum of evaporative cooling at the equator (Liu et al. 2005; Xie et al. 2010; Ying et al. 2016). However, there is lesser consensus on the zonal pattern of the equatorial Pacific SST response, as well as the physical mechanisms responsible for the pattern. While a majority of models in the Climate Model Intercomparison Project phase 5 (CMIP5) simulated a weakening of the zonal SST gradient along the equatorial Pacific in a warming climate, leading to an El Niño–like warming pattern (DiNezio et al. 2013; Ying et al. 2016; Coats and Karnauskas 2017; Plesca et al. 2018), some models simulated no change in the zonal SST gradient (Collins et al. 2005; Liu et al. 2005) or even a strengthening of the zonal SST gradient, i.e., a La Niña-like warming pattern (Cane et al. 1997; Seager and Murtugudde 1997; Fang and Wu 2008; Kohyama et al. 2017; Kohyama and Hartmann 2017). In addition, the historical simulations of CMIP models failed to reproduce the observed strengthening of the zonal SST gradients over the past several decades (Kociuba and Power 2015; Seager et al. 2022). This has been attributed to the lack of vigor in the simulated internal variability (Kosaka and Xie, 2013; England et al. 2014; Kociuba and Power 2015; Bordbar et al. 2017), and the lack of inter-basin interaction of SST change patterns (Wang 2006; Zhang et al. 2019; Cai et al. 2019; Wang 2019; Fosu et al. 2020). Therefore, it is important to enhance our understanding of the dominant mechanisms of equatorial Pacific SST changes and what causes such a large spread among the CMIP models. Moreover, studies also found that the response of the equatorial Pacific SST to global warming experiences a fast phase and a slow phase. The fast response is characterized with an enhanced zonal SST gradient, followed by a gradual transition to an El Niño–like pattern with time (Liu 1998; Luo et al. 2017; Heede et al. 2020, 2021).

Several distinct mechanisms have been proposed to explain the zonal structure of the equatorial Pacific SST warming pattern. The first is the weakened Walker cell mechanism that contributes to formation of the El Niño–like warming pattern (Vecchi et al. 2006; Vecchi and Soden, 2007), i.e., the weakened Walker circulation, which results from the reduced vertical mass flux in the tropical circulation (Held and Soden 2006), will reduce the zonal SST gradient by decreasing the cold upwelling in the equatorial eastern Pacific Ocean. Secondly, greater evaporative cooling over the warm pool than the cold tongue is also thought to be a mechanism that promotes the El Niño–like warming pattern (Knutson and Manabe 1995; Merlis and Schneider 2011; Lu and Zhao 2012; Ying et al. 2016). The cloud–shortwave-radiation–SST feedback is suggested to be another factor favoring the El Niño–like warming pattern (Ramanathan and Collins 1991; Ying et al. 2016), i.e. there is stronger decreased shortwave radiation over the western Pacific than the eastern Pacific that cools the former more. In addition, the oceanic tunnel mechanism can warm the water upwelled in the equatorial eastern Pacific, favoring an El Niño–like SST warming pattern. Specifically, there are two processes that adjust the temperature of water upwelled in the equatorial eastern Pacific through its connection with the extra-tropics. On the one hand, the extratropical warm SST anomalies in response to climate warming first subduct into the thermocline, then are transferred to the tropics within the subsurface branch of the Pacific subtropical cells (STCs), and eventually upwell to the surface in the equatorial eastern Pacific (McCreary and Lu 1994; Gu and Philander 1997; Rodgers et al. 2003; Burls et al. 2017). On the other hand, the reduction in the strength of the STCs could also warm the equatorial eastern Pacific by reducing the amount of cold thermocline water that upwells there (Kleeman et al. 1999; Yamanaka et al. 2015). Thus, the oceanic tunnel contains effects of both mean ocean circulation and ocean circulation change. Counter to the aforesaid mechanisms promoting the El Niño–like warming pattern, the background cold upwelling tends to give rise to a La Niña-like pattern by damping the SST warming in the equatorial eastern Pacific, which is known as the oceanic dynamical thermostat (ODT) mechanism (Clement et al. 1996; Seager and Murtugudde 1997; Vecchi et al. 2008).

Although all of these mechanisms mentioned above are theoretically reasonable, the jury is still out on their relative importance and potential interaction, as well as which mechanisms will ultimately dominate the formation of zonal warming pattern and the transition from the fast to slow response. Recently, the relative importance of different theories has been investigated using a sequence of model experiments (Luo et al. 2015; Luo et al. 2017; Seager et al. 2019; Heede et al. 2020; Heede et al. 2021). For example, Luo et al. (2015) applied an overriding technique in the ocean component of a climate model to isolate the role of ocean dynamical process from air–sea thermal interaction in tropical SST warming pattern formation. They found that the weakening of the equatorial easterlies contributes only 20% to the formation of El Niño-like SST warming. In other words, the mechanisms related to air–sea thermal interaction play a more important role than the weakened Walker cell mechanism. However, the role of ocean dynamical process has not been separated cleanly in their study, since the thermodynamic flux change can also drive ocean circulation change. Using a series of idealized CO_2 forcing experiments, Heede et al. (2020, 2021) investigated the relative importance of divergent mechanisms in equatorial Pacific SST warming patterns and tried to combine them into a coherent framework. They found that different patterns of the fast and slow responses can be attributed to different balance between mechanisms that counteract or amplify the ODT effect. In addition, they indicated that the shift from the fast to the slow response pattern is driven by both the increased extratropical warming being transported to the tropics by the mean STCs and a slowdown of the STCs itself, which is consistent with the results of Liu (1998) and Luo et al. (2017). However, the relative importance of the mean STCs and the slowdown of the STCs in the temporal evolution of the equatorial Pacific SST warming pattern is still unclear.

This study aims to address the relative roles of the oceanic and atmospheric processes in the formation of the equatorial Pacific SST warming pattern by precisely separating them. To this end, we use a set of purposely designed experiments in the Community Earth System Model

(CESM) by Garuba et al. (2018a). A tracer decomposition method (Banks and Gregory 2006; Xie and Vallis 2012) is applied to decompose the anomalous equatorial Pacific SST into atmosphere-forced and ocean-driven components, the former being forced by atmospheric processes (referred to as the *passive* component) and the latter driven by ocean circulation changes (referred to as the *active* component), respectively. Specifically, the contribution of the atmospheric processes to SST anomaly is isolated by disabling the effect of the ocean circulation changes on the temperature response and its feedback to the air-sea interaction, while the ocean-driven component is then obtained by subtracting the atmosphere-forced component from the total response. Compared with the study of Luo et al. (2015), in which ocean dynamical process is wind-driven only, the *active* component here contains the total contribution of ocean dynamical changes. This partial coupling technique has already been used to reveal the relative important roles of ocean and atmosphere in regulating climate sensitivity (Garuba et al. 2018a) and in driving Atlantic multidecadal variability (Garuba et al. 2018b), as well as in regulating the Southern Ocean heat uptake and storage (Li et al. 2022).

The rest of the paper is organized as follows. Section 2 describes the model experiments and metrics used in this study. Section 3 presents the quasi-equilibrium response and the temporal evolution of the SST response pattern in the equatorial Pacific, as well as the relative contributions of atmospheric and oceanic processes. Section 4 compares the warming patterns between the *passive* SST and the slab ocean SST response. Section 5 is a discussion and conclusion.

2 Model experiments and analysis methods

2.1 Coupled experiments

We use the output of the CESM experiments performed by Garuba et al. (2018a), which consist of three simulations (Table 1). First, a control simulation (CTRL) is integrated with no external forcing using the CESM, initialized from a 1000-year preindustrial simulation already existing at NCAR. Then, the fully and partially coupled simulations are branched out from the preindustrial control run, forced by abrupt CO_2 quadrupling. In the former (FULL), the standard atmosphere-ocean coupling is used. In the partially coupled experiment (PARTIAL), although the same bulk formula in the coupler is used for the air-sea thermal coupling, the effect of the SST anomalies due to the ocean circulation changes are suppressed in the surface coupling as the term *partial coupling* implies (see Section 2.1b for details). All three simulations are integrated for 150 years. Next, we explain how to isolate the ocean circulation feedback effect from the full climate change response through the comparison between FULL and PARTIAL experiments and the implementation of temperature-like tracers.

a. Fully coupled experiment

In FULL, the change of ocean temperature (T'_{OF}) response to external forcing can be expressed as:

$$\frac{DT'_{OF}}{Dt} = Q' - \boldsymbol{v}'_F \cdot \nabla\bar{T} \tag{1}$$

where Q' is the surface heat flux anomaly, T'_{OF} is ocean temperature anomaly, and $\boldsymbol{v}'_F$ is three-dimensional ocean circulation anomaly; subscript F denotes the variables in FULL; overbar represents the control value, and primes denote anomalies in response to external forcing; D/Dt is the total derivative, which consists of the time derivative and the advection due to the ocean circulation (i.e., $D/Dt = \partial/\partial t + \boldsymbol{v}\,\cdot$). Eq. (1) represents the ocean temperature anomaly that is caused by both the change in surface heat flux (Q') and the change in the ocean circulation through advecting the control ocean temperature field ($\boldsymbol{v}'_F \cdot \nabla\bar{T}$). Thus, we can partition the change of ocean temperature into two parts based on these forcing effects:

$$T'_{OF} = T'_{FS} + T'_{FD} \tag{2}$$

$$\frac{DT'_{FS}}{Dt} = Q' \tag{3}$$

$$\frac{DT'_{FD}}{Dt} = -\boldsymbol{v}'_F \cdot \nabla\bar{T} \tag{4}$$

T'_{FS} is referred to as the surface-forced component due to the surface heat flux anomaly Q', and T'_{FD} can be thought of as the dynamically induced component due to the ocean circulation change that advects the control ocean temperature field $\boldsymbol{v}'_F \cdot \nabla\bar{T}$.

To obtain T'_{FS} and T'_{FD} in FULL, two temperature-like tracers (P_1 and P_2) are introduced following Banks and Gregory (2006) and Xie and Vallis (2012). The first tracer P_1 is designed to represent the surface-forced ocean temperature anomaly (T'_{FS}). It is set to zero everywhere at initialization and is forced by the surface heat flux anomaly Q', which is constructed by subtracting the surface heat flux in CTRL from that in FULL (i.e., $Q' = Q - \bar{Q}$). The tracer P_1 so implemented satisfies Eq. (3) precisely and gives us the information of T'_{FS}. The second tracer P_2 is set to be the control ocean temperature $\bar{T}$ at initialization and forced by the baseline surface heat flux $\bar{Q}$ from CTRL. Since P_2 evolves along with a perturbed circulation $\bar{\boldsymbol{v}} + \boldsymbol{v}'_F$ rather than control circulation $\bar{\boldsymbol{v}}$, it will deviate from $\bar{T}$ with time because of ocean circulation changes $\boldsymbol{v}'_F$. The difference between tracer P_2 and $\bar{T}$ represents the dynamics-induced temperature anomaly (i.e., $T'_{FD} = P_2 - \bar{T}$). The sum of the two response components obtained by the two tracer approaches, i.e., $T'_{FS} + T'_{FD}$, agrees well with the total temperature anomaly (comparing Fig. 1a with 1b), validating the tracer approaches for decomposing the ocean temperature response in FULL.

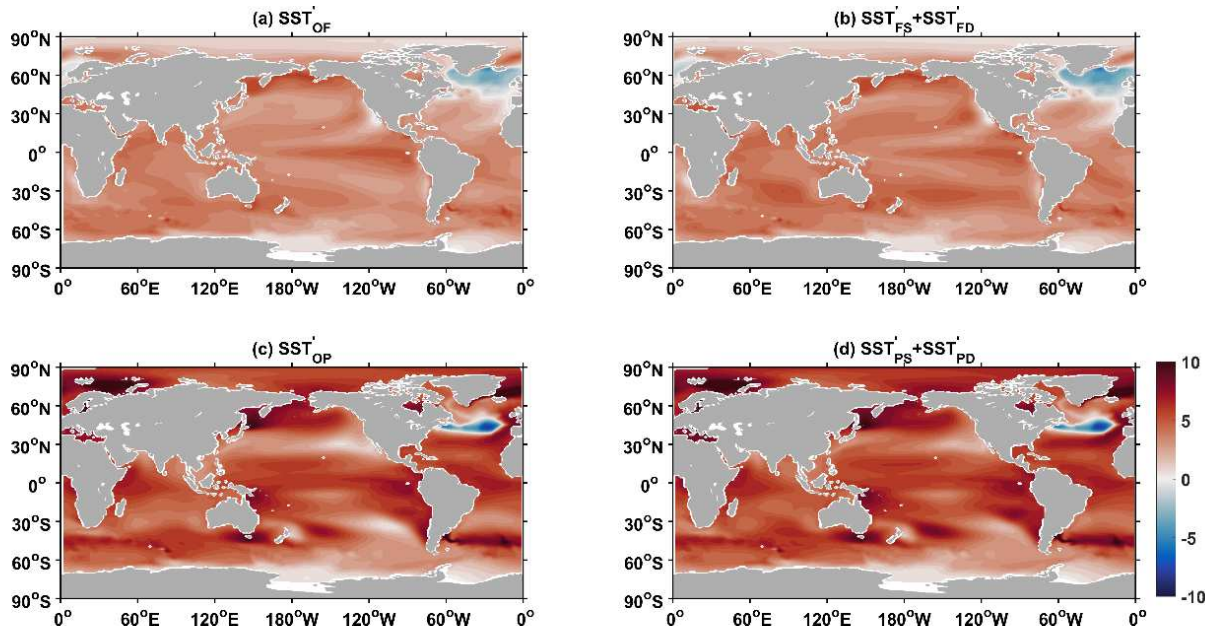

Fig. 1. Changes of SST (°C) in (a) the total response and (b) the sum of surface-forced and dynamically induced components in FULL. (c) and (d) are same as (a) and (b) but for the PARTIAL. A mean of the last 50 years of each simulation is used for analysis. The resemblance between the sum of tracers and the actual SST response supports the validity of the tracer approach.

However, there is a caveat in the decomposition above; the T'_{FS} component does not cleanly isolate the atmosphere-forced component from the ocean-driven one. To distinguish the purely atmosphere-forced component from the T'_{FS} component, and better delineate the concept of the former, we conceptually decompose the surface heat flux forcing for the tracer P_1 in FULL as follows:

$$Q' = \alpha(T'_{AF} - T'_{OF})|_s = \alpha(T'_{AF} - T'_{FS} - T'_{FD})|_s \quad (5)$$

where T'_{AF} is the atmospheric temperature anomaly, which is ultimately attributable to the CO_2 forcing and the response in the atmosphere; T'_{OF} is the oceanic temperature anomaly; $|_s$ represents surface values of the variables; α is the coupling coefficient (varying in space and time) that represents the strength of the coupling between the atmosphere and ocean. In practice, the surface heat flux forcing (Q') is calculated online by subtracting the baseline surface heat flux (computed from CTRL) from the total surface heat flux, which is calculated by the coupler of the model using the bulk formula. Eq. (5) proves to be a good approximation to the bulk formula used for the calculation of the surface heat flux anomaly (Haney 1971; Rahmstorf and Willebrand 1995; Rivin and Tziperman 1997; He et al. 2022). Eq. (5) shows the total surface heat flux anomaly (Q') is proportional to the difference between the surface atmospheric temperature anomaly and the SST anomaly, which itself is induced partly by the ocean circulation changes (i.e., $T'_{FD}|_s$). Therefore, in FULL the surface forcing responsible for T'_{FS} is not purely atmosphere-forced and the T'_{FS} component has been indirectly affected by ocean circulation changes. As a result, there is an inconsistency between the so-called surface-forced component (T'_{FS}) and the surface heat flux anomaly (Q'), and a causal relationship is attempted to be established between the two.

Given this caveat, there is a need to design a cleaner decomposition method to separate the *active*, ocean-driven temperature anomaly (T'_{active}) from the *passive*, purely atmosphere-forced anomaly ($T'_{passive}$). The key to isolate the purely atmosphere-forced temperature response is to remove the ocean-forced component from the surface heat flux anomaly: to decompose the surface heat flux anomaly (Q') into a passive component ($Q'_{passive}$) caused directly by atmospheric CO_2 increase and an active component (Q'_{active}) caused indirectly by ocean circulation change, i.e., $Q' = Q'_{passive} + Q'_{active}$. To this end, a novel partial coupling technique is employed to configure a case where the surface heat flux change under CO_2 forcing is purely atmospherically-induced so that the *passive* surface heat flux anomaly can be isolated from the *active* one. A recapitulation of the partial coupling approach is provided as follows, and interested readers are referred to Garuba et al. (2018a) and Garuba and Rasch (2020) for further technical details.

b. Partially coupled experiment

As demonstrated in Garuba et al. (2018a) and Garuba and Rasch (2020), a consistent isolation of the purely surface-forced, *passive* temperature response is achievable in a partially coupled configuration, wherein the surface heat flux anomaly is the result of partial coupling to the surface-forced component of the ocean temperature anomaly, which itself is solely forced by the *passive* surface heat flux anomaly. To realize this consistency, a surface-forced temperature tracer T'_{PS} is introduced to be only subject to the *passive* surface flux anomaly formulated as:

$$Q'_{passive} = \alpha(T'_{AP} - T'_{PS})|_s \tag{6}$$

where T'_{AP} is the atmospheric temperature anomaly, which is induced by CO_2 increase. And the evolution of T'_{PS} is governed by:

$$\frac{DT'_{PS}}{Dt} = Q'_{passive} \tag{7}$$

In the actual execution of the partial coupling, the $T'_{PS}|_s$ is added to the baseline SST (computed from CTRL run) and the resulted value is then used to substitute the SST into the bulk formula to compute the surface heat flux. The resultant surface heat flux provides the actual thermal interaction between the atmosphere and the ocean in PARTIAL (i.e., $Q_P = \bar{Q} + Q'_{passive}$). In addition, the temperature-like tracer P_1 is introduced to diagnose T'_{PS}, which is set to zero at initialization and subject to the forcing of the surface heat flux anomaly (i.e., $Q'_{passive}$). Like in the FULL, the ocean temperature anomaly in PARTIAL can also be decomposed into surface-forced and dynamically induced components (i.e., $T'_{OP} = T'_{PS} + T'_{PD}$, subscript P denotes the variables in PARTIAL), and the validity of the tracer approach is verified by the good agreement between the sum of the two tracers and the actual SST response (comparing Fig. 1c with 1d).

As such, a better consistency is achieved in PARTIAL between the surface heat flux anomaly ($Q'_{passive}$) and the surface-forced ocean temperature tracer (T'_{PS}) (comparing to the fully-coupled counterpart Eqs. (3) and (5)). In other word, the surface-forced ocean temperature (T'_{PS}) in the PARTIAL is entirely atmosphere-originated and can be referred to as the *passive* component ($T'_{passive}$) in the context of this study, which can be expressed as:

$$\frac{DT'_{passive}}{Dt} = Q'_{passive} \tag{8}$$

By corollary, the active component due to the ocean circulation adjustment to CO_2 forcing can be inferred as the difference between the total temperature anomaly (T'_{OF}) in FULL and $T'_{passive}$ in PARTIAL, and it will be referred to as the *active* component (T'_{active}) hereafter. Its evolution can be derived from Eq. (1) minus Eq. (8):

$$\frac{DT'_{active}}{Dt} = Q'_{active} - \boldsymbol{v}'_F \cdot \nabla\overline{T} \tag{9}$$

As implied by Eq. (9), T'_{active} can be understood as the response to the direct effect of the ocean circulation change through advecting the mean temperature ($\boldsymbol{v}'_F \cdot \nabla\overline{T}$) plus the response to the indirect effect due to the surface heat flux anomalies (Q'_{active}) induced by the ocean circulation change.

In summary, through the fully and partially coupled experiments, we construct a clean decomposition framework as expressed by Eqs. (8)-(9), which affords an interpretation of the full CO_2-forced response as the sum of the atmosphere-forced component (or *passive* component: $T'_{passive}$ and $Q'_{passive}$) and the ocean circulation change-driven component (or *active* component: T'_{active} and Q'_{active}). The key advantage of this approach over the conventional implementation of a tracer (Banks and Gregory, 2006; Xie and Vallis, 2012) is that the ocean temperature response and the surface flux anomaly are self-consistent in both FULL and PARTIAL experiments, so are the differences between the two experiments. The validity of the *active* component derived from linearly subtracting the PARTIAL from the FULL has been demonstrated by Garuba and Rasch (2020), who performed an additional ocean-driven partially coupled simulation to obtain the *active* component directly, showing that the total response in the fully coupled experiment can be recovered from the sum of the *active* and *passive* components simulated separately.

Table 1: Model experiments with CESM1

Name	Run (yrs)	Description
Coupled simulations		
CTRL	150	Control fully coupled simulation (Preindustrial CO_2)
FULL	150	Perturbed fully coupled simulation (4×CO_2)
PARTIAL	150	Perturbed partially coupled simulation (4×CO_2)
Slab ocean simulations		
CTRL-slab	90	Control slab ocean simulation (Preindustrial CO_2)
4×CO_2-slab	90	Perturbed slab ocean simulation (4×CO_2)

2.2 Slab ocean experiments

To further verify the role of the atmospheric processes in ocean temperature response isolated using the PARTIAL, we use a slab ocean version of CESM (CESM-SOM) to investigate the tropical Pacific SST warming pattern. In the CESM-SOM, the ocean and atmosphere are only thermodynamically coupled, and SST is computed from surface heat flux and prescribed ocean energy flux divergence (Q-flux). Both the slab ocean control run (CTRL-slab) and perturbation run (4xCO_2-slab) are integrated for 90 years (Table 1), in which the mixed layer depth and Q-flux are both derived from the climatology of CTRL simulation. A mean of the last 20 years of the model integration is used for our analysis in this study.

The ocean temperature response obtained from the slab ocean experiment can help to circumstantially validate the results of the partially coupled experiment, since both the partially coupled experiment and slab ocean experiment are designed to isolate the role of atmospheric processes, but with some notable differences. In the partially coupled experiment, the mean ocean circulation acting on the ocean temperature anomaly produces anomalous ocean heat convergence, which, however, is excluded in the slab ocean model. Hence, by comparing the ocean temperature response between these two experiments, we can infer the effect of anomalous ocean heat convergence on the ocean temperature response due to the mean ocean circulation advection (such as the ODT effect).

2.3 Mixed layer heat budget analysis

The formation mechanisms of the equatorial Pacific SST warming pattern have been studied with the heat budget analysis in many previous studies (DiNezio et al. 2009; Luo et al. 2015,2017; Liu et al. 2017; Ying et al. 2016). Following DiNezio et al. (2009) and Xie et al. (2010), the heat budget can be computed by vertically integrating the temperature equation over mixed layer:

$$\frac{\partial Q}{\partial t} = Q_{net} + D_O + R \quad (10)$$

where $\frac{\partial Q}{\partial t}$ is the vertically integrated heat storage rate; Q_{net} is the net surface heat flux obtained by subtracting the radiative flux at the bottom of the mixed layer from the surface heat flux, and it is comprised of the longwave radiation (Q_{LW}), shortwave radiation (Q_{SW}), latent heat flux (Q_E), and sensible heat flux (Q_H); D_O represents the ocean heat transport; *R* is the residual term, which includes sub-grid scale processes (e.g., vertical mixing and lateral entrainment). D_O can be decomposed as:

$$D_O = Q_u + Q_v + Q_w \quad (11)$$

where Q_u , Q_v and Q_w represent the zonal, meridional and vertical ocean heat transport divergences, respectively. The sum of D_O and *R* represent the total effect of ocean dynamical processes.

For an equilibrium state, the heat storage rate is negligible, so the right-hand side of Eq. (10) is zero. The heat budget is thus balanced between the surface heat flux and the ocean dynamical processes:

$$Q_{LW} + Q_{SW} + Q_E + Q_H + Q_u + Q_v + Q_w + R = 0 \quad (12)$$

A change of each term in Eq. (12) in response to quadrupled CO_2 represents the effect of different mechanism in modifying SST. For example, the latent heat change (ΔQ_E) represents the effect of evaporative cooling, the shortwave radiation change (ΔQ_{SW}) indicates the effect of cloud–shortwave-radiation–SST feedback, and the effect of the ODT can be implied in the vertical ocean heat transport divergence (ΔQ_w).

Furthermore, since the terms of ΔQ_u, ΔQ_v and ΔQ_w include both the effects of ocean circulation change and ocean temperature gradient change, which are associated with different mechanisms, we decompose the changes of ocean heat transport divergence into three parts:

$$\begin{aligned}\Delta Q_u &= -\rho_0 \mathrm{C}_p \int_{-H}^{0} u \frac{\partial \Delta T}{\partial x} dz - \rho_0 \mathrm{C}_p \int_{-H}^{0} \Delta u \frac{\partial T}{\partial x} dz - \rho_0 \mathrm{C}_p \int_{-H}^{0} \Delta u \frac{\partial \Delta T}{\partial x} dz \\ &= \Delta Q_{u1} + \Delta Q_{u2} + \Delta Q_{u3} \end{aligned} \tag{13}$$

$$\begin{aligned}\Delta Q_v &= -\rho_0 \mathrm{C}_p \int_{-H}^{0} v \frac{\partial \Delta T}{\partial y} dz - \rho_0 \mathrm{C}_p \int_{-H}^{0} \Delta v \frac{\partial T}{\partial y} dz - \rho_0 \mathrm{C}_p \int_{-H}^{0} \Delta v \frac{\partial \Delta T}{\partial y} dz \\ &= \Delta Q_{v1} + \Delta Q_{v2} + \Delta Q_{v3} \end{aligned} \tag{14}$$

$$\begin{aligned}\Delta Q_w &= -\rho_0 \mathrm{C}_p \int_{-H}^{0} w \frac{\partial \Delta T}{\partial z} dz - \rho_0 \mathrm{C}_p \int_{-H}^{0} \Delta w \frac{\partial T}{\partial z} dz - \rho_0 \mathrm{C}_p \int_{-H}^{0} \Delta w \frac{\partial \Delta T}{\partial z} dz \\ &= \Delta Q_{w1} + \Delta Q_{w2} + \Delta Q_{w3} \end{aligned} \tag{15}$$

where ρ_0 is seawater density; C_p is seawater specific heat; *H* denotes the mixed layer depth, which is chosen as a constant of 55 m following Luo et al. (2015) and Liu et al. (2017); *T* is ocean temperature in the control simulation (i.e., $T = \bar{T}$); u, v, w are zonal, meridional and vertical ocean currents in the control simulation, respectively; Δ denotes the difference of variables between the fully coupled and control simulations (i.e., $\Delta T = T'_{OF}$). ΔQ_{u1}, ΔQ_{v1} and ΔQ_{w1} represent the advection of the temperature anomalies by the mean ocean circulation. ΔQ_{u2}, ΔQ_{v2} and ΔQ_{w2} represent the advection of the mean temperature by the ocean circulation anomalies. ΔQ_{u3}, ΔQ_{v3} and ΔQ_{w3} are the non-linear terms, representing the interactions between ocean circulation changes and ocean temperature gradient changes. The mixed layer heat budget in FULL helps to verify the effects of ocean circulation changes in the temperature response that have been clearly isolated through the FULL and PARTIAL experiments (i.e., the *active* component) and to quantify the relative importance of each of the identified processes.

3 Results

3.1 The SST response at the quasi-equilibrium stage

We first examine the quasi-equilibrium pattern of SST over the tropical Pacific in response to quadrupled CO_2. Since the SST anomalies stabilize after 100 years of integration (not shown), a mean of the model years of 101-150 is taken to represent the quasi-equilibrium response in this section. The total response of the tropical Pacific SST is characterized by an El Niño-like warming pattern in the equator and a minimum warming in the southeastern subtropics (Fig. 1a), which are broadly consistent with previous studies (Meehl et al. 2007; Lu et al. 2008; Xie et al. 2010; DiNezio et al. 2013; Kociuba and Power 2015; Luo et al. 2015; Ying et al. 2016; Coats and Karnauskas 2017; Plesca et al. 2018). Making use of the fully and partially coupled experiments (Table 1), we decompose the total SST response into the atmosphere-forced *passive* component (Fig. 2b) and ocean-dynamically induced *active* component (Fig. 2c). It is found that, although the *passive* SST change in the tropical Pacific is characterized by a greater warming north of the equator than south of the equator and a minimum warming in the southeastern subtropics, it is nearly uniform warming along the equator and thus has no contribution to the El Niño-like warming pattern. On the contrary, the *active* SST change is featured with a cooling in the western equator but a warming in the central and eastern equator, resulting in a decreased SST zonal gradient along the equator and thus an El Niño-like warming pattern. Therefore, the decomposition indicates that the El Niño-like SST warming pattern is predominantly the result of ocean circulation changes, while the atmospheric processes have no contribution. To further demonstrate the dominant role of ocean dynamical processes for the El Niño-like warming pattern formation, we calculate the regional mean of SST anomalies in western equatorial Pacific (WEP; 5°S–5°N, 130°E–180°), central and eastern equatorial Pacific (CEP; 5°S–5°N, 160°–100°W), and the difference between them (Fig. 2d). It is found that, while the total warming of SST in both WEP and CEP (left and middle gray bars in Fig. 2d) is dominated by the *passive* component (left and middle red bars in Fig. 2d), the decreased zonal gradient of SST (right gray bar in Fig. 2d) is almost solely determined by the *active* component (right blue bar in Fig. 2d).

As reviewed in the introduction, Luo et al. (2015) have found that the weakening of the equatorial easterlies contributes only 20% to the El Niño-like SST warming. Hence, they concluded that the role of ocean dynamical process is feeble in the formation of El Niño-like warming pattern. However, the contribution of ocean dynamics has not been fully isolated from the contribution of the thermal warming effect in their study, since the latter can also lead to an ocean circulation change. In this study, we can isolate the effect of total ocean circulation change (the *active* component) from the total tropical SST response to global warming. It is found that the El Niño-like SST warming pattern over the equatorial Pacific is determined entirely by the total effect of ocean circulation change (Fig. 2c). Therefore, in combination with the modeling result of Luo et al. (2015), we can conclude that the ocean circulation changes induced by both buoyancy fluxes and wind stress play positive roles in the El Niño-like warming pattern, but the former is clearly dominant over the latter. In fact, the importance of buoyancy fluxes in changing the Pacific tropical ocean circulation has been identified with the help of the overriding technique in previous studies (Luo et al. 2015; Liu et al. 2017). For example, in response to global warming, the STC weakening was found to be mainly driven by more stratified subtropical ocean induced by buoyancy flux changes.

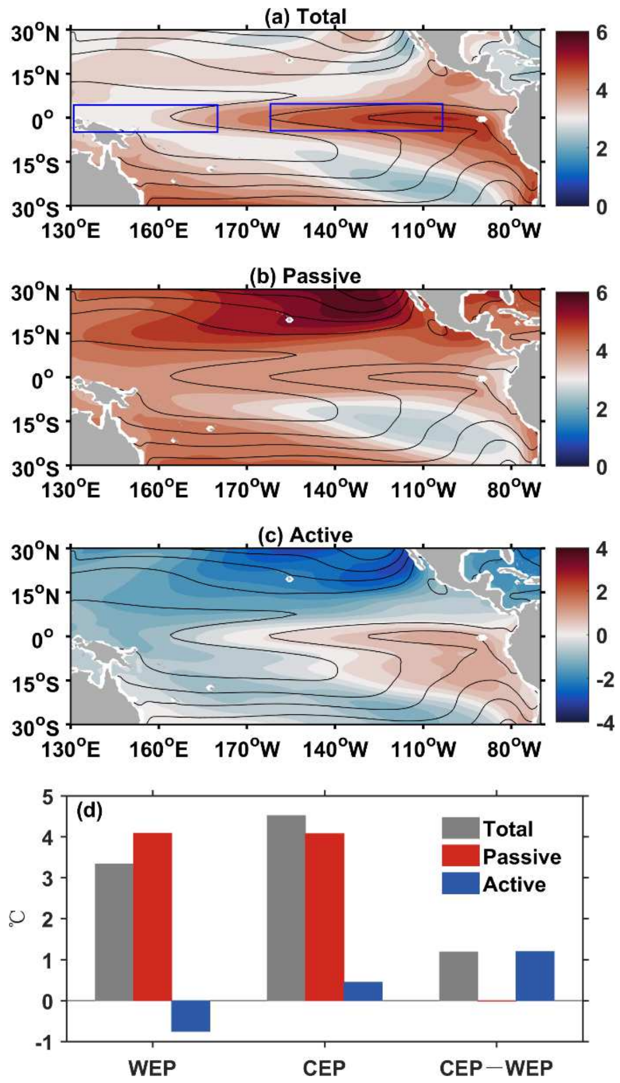

Fig. 2. Changes of SST (°C) in (a) the total response and its (b) passive and (c) active components. Superimposed is the mean SST field in CTRL (contour interval (CI) = 2 °C). The boxes in (a) represent the western equatorial Pacific (WEP; 5°S–5°N, 130°E–180°) and the central and eastern equatorial Pacific (CEP; 5°S–5°N, 160°–100°W) regions, respectively. (d) Changes of SST in the WEP and CEP as well as their differences (CEP minus WEP) in the total response (grey bars) and its passive (red bars) and active (blue bars) components.

Next, we examine the changes in surface heat flux and its *passive* and *active* components (Fig. 3). The total change in the surface heat flux includes a heat loss along the equator and in the southeast subtropics, which is dominated by its *active* component (comparing Figs. 3a with 3c). In addition, there is an intriguing cancellation in the surface flux response between the passive and the active components along the equator. The maximum warming in the eastern equator corresponds to the maximum surface heat flux loss (comparing Figs. 2a with 3a), suggesting a damping role of the surface heat flux in the equatorial Pacific SST warming. This further verifies the decisive role of the ocean dynamical change in the formation of the El Niño-like SST warming along the equator. The *passive* heat flux change includes a large heat gain in the central and eastern equatorial regions as well as the zonal band around 10°N, and a large heat loss in the southeast subtropics (Fig. 3b), which explains the minimum warming there (Fig. 2b). However, the *passive* SST response is zonally uniform along the equator despite the stronger heat gain in the equatorial eastern Pacific. This mismatch between the atmosphere-forced surface heat flux change and SST response pattern alludes to ocean heat divergence caused by the mean ocean circulation, which will be discussed in detail next.

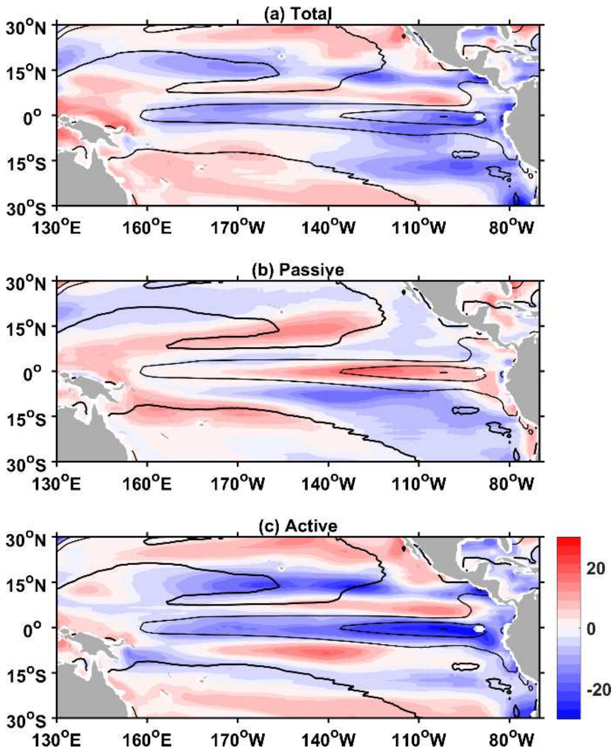

Fig. 3. Changes of surface heat flux (W m^{-2}) in (a) the total response and its (b) passive and (c) active components. Superimposed is the mean surface heat flux field in CTRL (CI = 50 W m^{-2}).

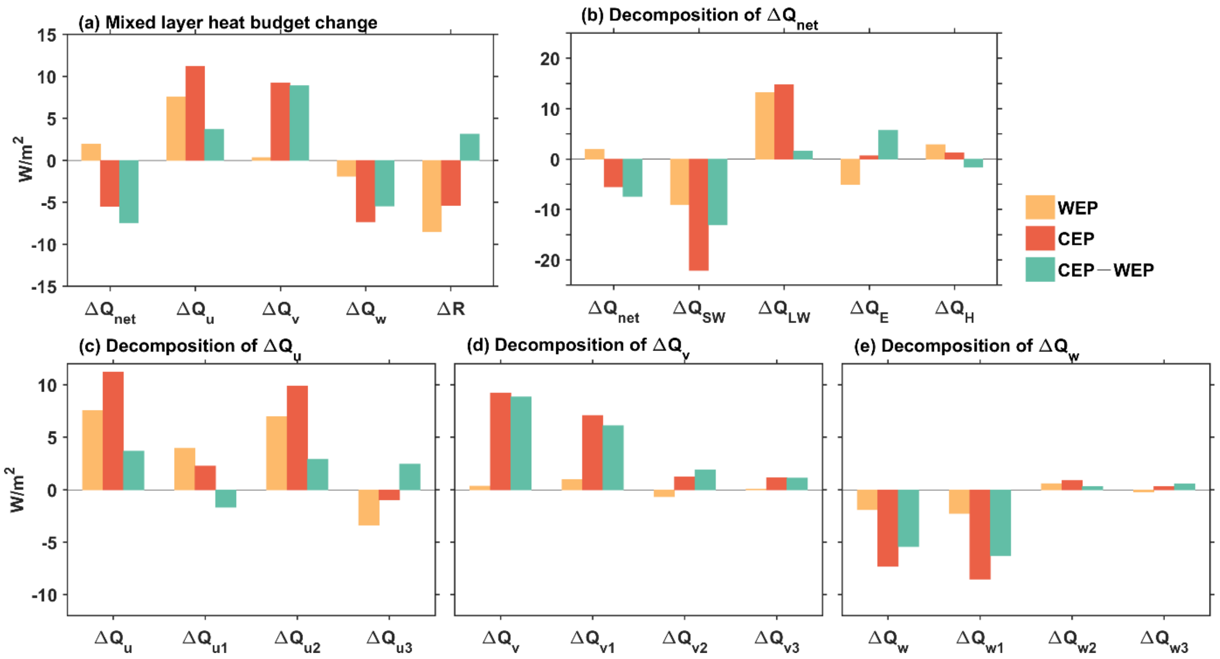

Fig. 4. Changes in the mixed layer heat budget in response to quadrupled CO_2 in FULL: (a) net surface heat flux (ΔQ_{net}), zonal heat transport divergence (ΔQ_u), meridional heat transport divergence (ΔQ_v), vertical heat transport divergence (ΔQ_w), and the residual (ΔR); (b) a decomposition of changes in the surface heat flux into latent heat flux (ΔQ_E), sensible heat flux (ΔQ_H), shortwave radiation (ΔQ_{SW}), and longwave radiation (ΔQ_{LW}). (c)-(e) a decomposition of changes in the zonal, meridional and vertical heat transport divergence into components associated with effects of temperature gradient changes (ΔQ_{u1}, ΔQ_{v1}, ΔQ_{w1}), ocean circulation changes (ΔQ_{u2}, ΔQ_{v2}, ΔQ_{w2}), and their nonlinear interactions (ΔQ_{u3}, ΔQ_{v3}, ΔQ_{w3}). Orange, red, and green bars represent the changes in WEP and CEP regions as well as their differences (CEP minus WEP), respectively.

To elucidate the particular oceanic processes that maintain the equatorial Pacific warming pattern in response to quadrupled CO_2, we apply the mixed layer heat budget analysis in FULL. We calculate the regional mean of heat budget in WEP and CEP, and use the difference between them for the budget of the zonal SST gradient. The positive term over the WEP and CEP represents the process that warms the SST there (red and orange bars in Fig. 4). Since the climatological value of CEP－WEP is negative, a positive change of CEP－WEP represents a decrease in the zonal SST gradient (green bars in Fig. 4). The result shows that the warming in the WEP (orange bars in Fig. 4a) is dominated by a decrease in the zonal heat convergence, which is damped by the heat transport from the residual term. For the CEP, both the zonal and meridional heat divergence changes contribute to its warming, while the heat divergence changes from the vertical advection and the residual term play a cooling role (red bars in Fig.

4a). Regarding the decrease in the zonal SST gradient (i.e., positive change of CEP－WEP) that we are more interested in, the main contribution comes from changes in the zonal and meridional heat transport divergence, with non-negligible contribution from a change in the heat divergence from the residual term, while both changes in the surface heat flux and vertical heat transport divergence contribute negatively to the decrease in the zonal SST gradient (green bars in Fig. 4a).

The zonal, meridional and vertical heat transport divergence changes are further decomposed into components associated with temperature gradient changes (ΔQ_{u1}, ΔQ_{v1}, and ΔQ_{w1}), ocean circulation changes (ΔQ_{u2}, ΔQ_{v2}, and ΔQ_{w2}), and their nonlinear interactions (ΔQ_{u3}, ΔQ_{v3}, and ΔQ_{w3}). Results show that the ocean circulation changes in all three directions act to decrease the zonal gradient of SST (the third green bars from the left in Figs. 4c-4d), favoring the El Niño-like warming pattern. This corroborates our previous conclusion that the decreased zonal gradient of SST is determined by its *active* component. Specifically, the eastward zonal current anomaly (Fig. 5a) induced by the weakened equatorial easterly (Fig. 5b) warms the eastern equatorial ocean by transporting more warm water from the warm pool to the cold tongue. Meanwhile, the weakened easterly produces less Ekman transport away from the equator and thus leads to an increase of SST in the eastern equator. Interestingly, the reduced upwelling over the equatorial eastern Pacific (Fig. 6b) also plays a role in warming the surface water there. In addition, the change in the meridional temperature gradient (ΔQ_{v1}) also contributes significantly to the SST warming in the eastern Pacific. In contrast, the most prominent damping effect on the El Niño-like warming pattern stems from the heat transport divergence due to the change in vertical temperature gradient (ΔQ_{w1}), which has been referred to as the ODT effect in the literature (Cane et al. 1997; Seager and Murtugudde 1997; An and Im, 2014). This is caused by an intensified stratification of the equatorial ocean in response to the quadrupled CO_2 (shading in Fig. 6a). Overall, the negative contribution of the ODT effect (ΔQ_{w1}) on the El Niño-like warming pattern overcompensates the positive contribution by ΔQ_{v1}, the total effect of the ocean temperature gradient changes is to hinder the El Niño-like warming pattern. The results of our budget analysis are consistent with previous studies (DiNezio et al.

2009; Luo et al. 2015; Ying et al. 2016). A new finding here is that it is the cooling effect of ODT due to the background upwelling (the second red bar from the left in Fig. 4e) that primarily compensates the warming effect of the *passive* surface heat flux (Fig. 3b) in the eastern equatorial Pacific, leading to a zonally uniform warming along the equator in the *passive* SST response (Fig. 2b), while the ocean heat transport divergence due to the zonal and meridional temperature gradient change also plays an important role.

Further examination of the surface heat flux (Fig. 4b) reveals its damping effect on the El Niño-like SST gradient, implying that surface heat flux mainly works to damp the ocean dynamically induced SST pattern over the equatorial Pacific. More specifically, this damping effect stems mainly from shortwave radiative flux (ΔQ_{SW}), the effect of which is partly compensated by the longwave radiative flux and the latent heat flux. The latent heat flux change can be decomposed into four major terms associated with the change of SST, the change of wind speed, the change of relative humidity, and the change of air-sea surface temperature difference, respectively (Du and Xie 2008; Richter and Xie 2008; Xie et al. 2010; Luo et al. 2017). It is found that the latent heat flux change is dominated by the change of wind speed (SST) over the CEP (WEP) region (not shown). The decrease of the shortwave radiative flux in the equatorial Pacific can be attributed mainly to the negative cloud–shortwave-radiation–SST feedback there. Moreover, this negative feedback is greater in the CEP than in the WEP due to the eastward shift of convective clouds (not shown).

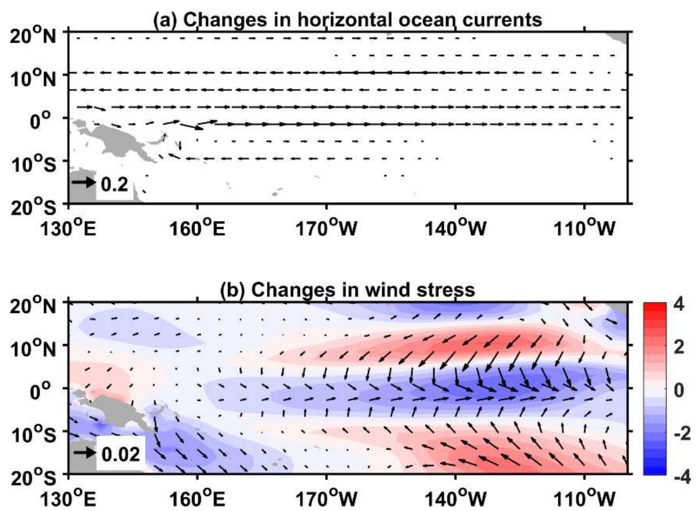

Fig. 5. (a) Changes in horizontal ocean currents averaged over the top 50 m (m s^{-1}). (b) Changes of wind stress (vectors) and its magnitude (color; 10^{-2} N m^{-2}).

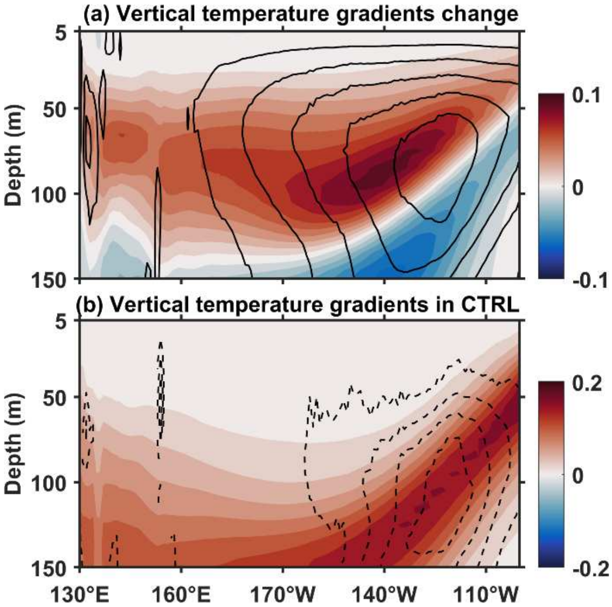

Fig. 6. (a) Changes of equatorial (averaged between 5°S-5°N) vertical temperature gradients (shading; °C m^{-1}) in response to quadrupled CO_2 and equatorial vertical velocity in CTRL (contours; CI = 2×10^{-6} m/s). (b) The equatorial vertical temperature gradients in CTRL (shading; °C m^{-1}) and changes of equatorial vertical velocity (contours; CI = 1×10^{-6} m/s) in response to quadrupled CO_2. The solid and dashed lines indicate upwelling and downwelling, respectively.

In summary, the results of fully and partially coupled experiments illustrate that the El Niño-like SST warming pattern over the equatorial Pacific is entirely induced by the effect of ocean dynamic changes (Fig. 2c). Making use of the mixed layer heat budget analysis, we find that the zonal and meridional ocean circulation changes play a dominant role for the formation of the El Niño-like warming pattern, with the vertical circulation change making a minor contribution. In addition, the air–sea interaction without the ocean dynamical feedbacks results in a zonally uniform warming in the *passive* SST response (Fig. 2b), which can be explained by the close balance between the total effect due to the mean advection (especially the ODT effect) and the effect of *passive* surface heat uptake. This result suggests that the ODT effect in shaping the ultimate spatial pattern of the equatorial Pacific SST response to global warming is weaker than previously thought.

3.2 The temporal evolution of SST response

In this section, we investigate the temporal evolution of the SST response pattern in the equatorial Pacific. Figure 7 shows the SST anomaly along the equator in different phases of response to quadrupled CO_2 as well as its *passive* and *active* components. Note that the areal mean increase of SST in the equatorial Pacific (5°S–5°N, 120°E-80°W) is removed to highlight the zonal SST gradient change. Consistent with previous studies (Liu 1998; Luo et al. 2017; Heede et al. 2020, 2021), there is an increase of the zonal SST gradient along the equator during the initial stage, followed by a weakening of this SST gradient when the system moves toward equilibrium (Fig. 7a). By decomposing the total SST response into the atmosphere-forced *passive* component and ocean-dynamically induced *active* component, we find that the temporal evolution of the equatorial SST response is almost entirely determined by the latter (comparing Figs. 7c with 7a). In other words, the temporal evolution of equatorial Pacific SST response is controlled by the ocean circulation changes. The *passive* component contributes little to the temporal evolution of equatorial Pacific SST response, as the *passive* SST anomalies are always zonally uniform along the equator (Fig. 7b).

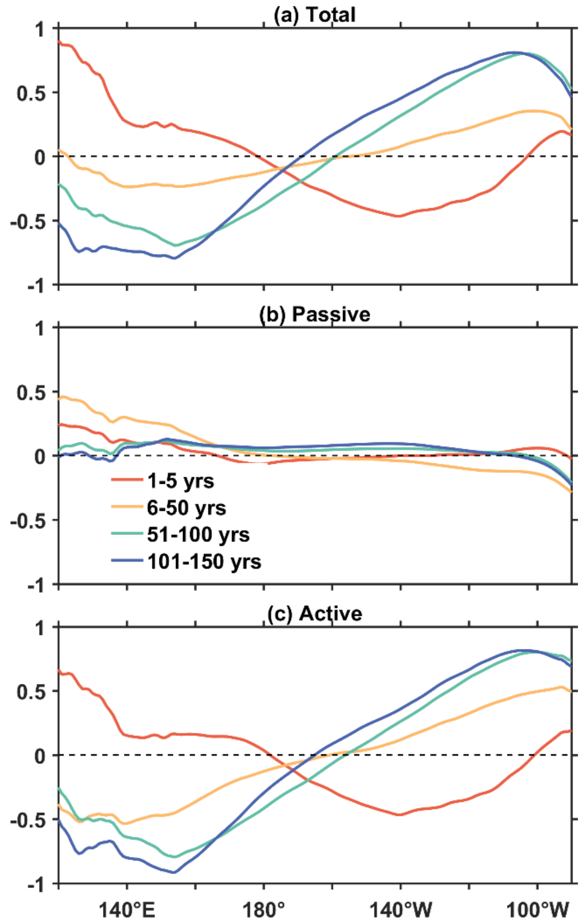

Fig. 7. (a) Zonal distribution of SST changes (°C) along the equator (5°S–5°N averaged, and the equatorial Pacific mean has been removed) in different phases of response to quadrupled CO_2 (red lines for years 1-5, yellow lines for years 6-50, green lines for years 51-100, and blue lines for years 101-150) and its (b) passive, and (c) active components.

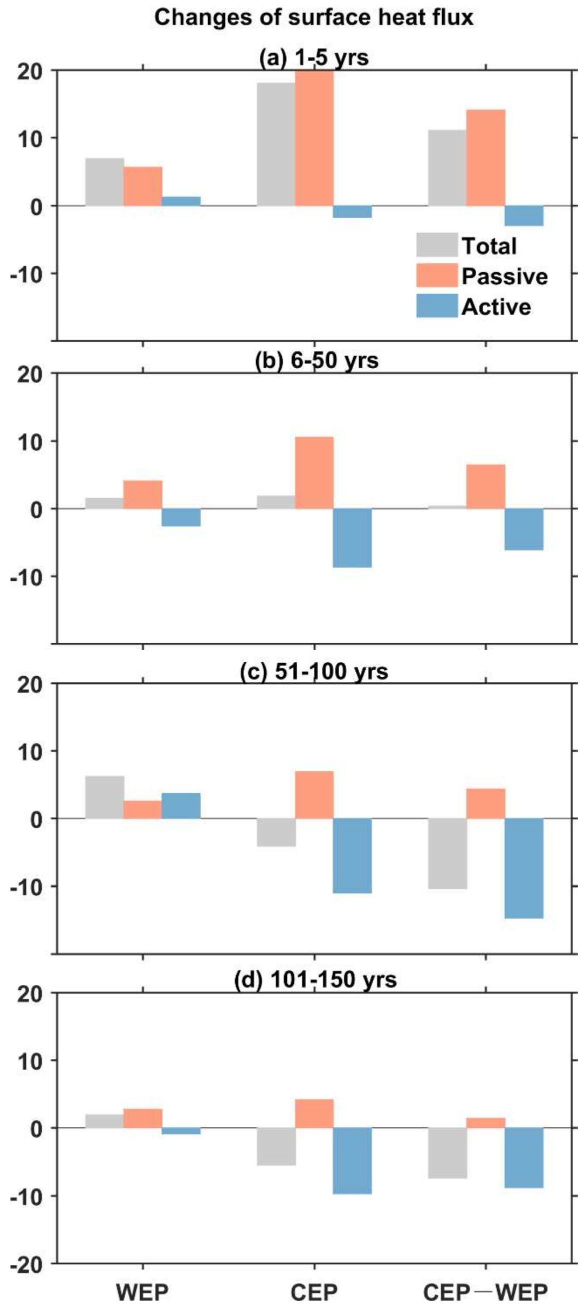

Fig. 8. Changes of surface heat flux (W m^{-2}) over the WEP and CEP regions as well as their differences (CEP minus WEP) in different phases of response to quadrupled CO_2: (a) years 1-5, (b) years 6-50, (c) years 51-100, and (d) years 101-150. The grey, orange and blue bars represent the total response, its passive, and its active components, respectively.

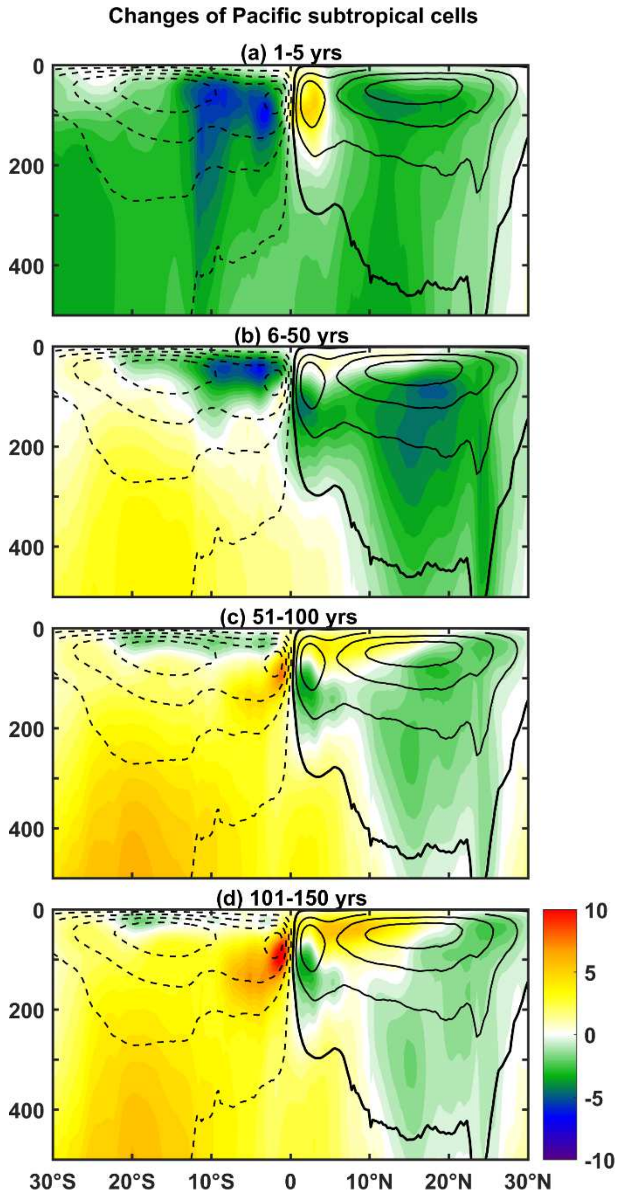

Fig. 9. Changes of the Pacific subtropical cells (STCs; Sv) in different phases of response to quadrupled CO_2: (a) years 1-5, (b) years 6-50, (c) years 51-100, and (d) years 101-150. The superimposed contours are the mean STCs in CTRL averaged over years 101-150 (solid and dashed lines for clockwise and anticlockwise circulations, respectively; CI = 8 Sv).

Figure 8 shows the changes of the surface heat flux in different stages over the WEP and CEP regions, as well as their gradients. The *active* surface heat flux change over the CEP region is negative during all time periods (middle blue bars in Fig. 8), so it cannot explain the gradual warming of the *active* SST over time in the CEP region (Fig. 7c). Hence, it is the ocean circulation change itself, rather than the *active* surface heat flux change, that is responsible for the temporal evolution of equatorial Pacific SST response pattern. This result, combining with previous studies (e.g., Liu 1998; Heede et al. 2020, 2021), suggests that the changes in the STCs play a significant role for the temporal evolution of equatorial Pacific SST warming pattern. Figure 9 shows the STC changes during different stages in response to CO_2 forcing. Under the warming, the STCs is found to slowdown in the northern hemisphere in all stages, but accelerate during the initial stage and then decelerate during the later stage in the southern hemisphere (Figs. 9a and 9b). The strength of the STCs stabilizes after 50 years of model integration in both hemispheres (Figs. 9c and 9d). Since the STCs transports warmer water out of the tropics within the surface layer and brings subsurface colder water to the surface in the eastern equatorial Pacific (McCreary and Lu 1994), its slowdown will cause a warming in the cold tongue region and thus a decrease of the zonal SST gradient. In addition, as pointed out by Luo et al. (2005), since there is a potential vorticity island in the northern tropics that blocks the connection between the equator and the northern subtropics, the influence from the southern STC appears to be more direct. Therefore, the temporal evolution of the STCs, especially its southern branch, accounts for the temporal evolution of the *active* SST along the equator. Specifically, the switch of the sign of the zonal SST gradient anomaly (red and yellow lines in Fig. 7c) appears to be synchronized with the opposite change of the STC in the southern hemisphere in the first two stages (Figs. 9a and 9b). After 50 years when the strength of the STCs is relatively stabilized (Figs. 9c and 9d), the zonal gradient of SST along the equator appears to level off (blue and green lines in Fig. 7c). According to previous studies (Luo et al. 2015; Liu et al. 2017), the response of the STCs to global warming is determined by both effects of the wind stress change and the buoyancy flux change. In particular, the weaker (stronger) trade winds can weaken (strengthen) the STCs. In addition, the increased upper ocean stratification over the subtropical Pacific may weaken the STCs by reducing water subduction. Thus, the shift of the southern STC change in the first two phases is mainly associated with the decrease of the easterly anomaly in the South Pacific and the increase of the upper-ocean stratification over the subtropical Pacific. Specifically, the wind-driven intensification of the southern STC overwhelms its reduction caused by increased upper-ocean stratification, resulting in an initial acceleration of the southern STC. Subsequently, the wind-driven acceleration of the southern

STC weakens significantly along with the weakening of the easterly anomaly in the South Pacific. The southern STC begins to decelerate as the buoyancy flux change plays a more dominant role.

This result is different from the earlier conclusion from passive tracer experiment with an ocean-alone model in Luo et al. (2017), who found that the decrease of SST zonal gradient change with time results largely from the passive advection of global warming-induced warmer extratropical waters by mean STCs. We believe that much of this discrepancy is to do with how the surface flux is treated in the passive tracer experiments using an ocean-alone model versus a coupled climate model. In the ocean-alone experiment, the passive tracer is restored to a constant surface temperature anomaly, so the realized "passive" surface temperature is the result of the heat balance between the restoration flux and the advection effect of the mean ocean circulation, and the pattern of the tracer is determined by the spatial distribution of the mean ocean circulation. In the PARTIAL used in this study, however, the *passive* surface heat flux change is "self-induced" by the *passive* ocean temperature warming, meanwhile subject to atmospheric adjustment. Due to the interactive atmosphere, both the atmospheric feedbacks and the mean ocean circulation determine the pattern of the tracer. In the CEP, the warming effect of the *passive* surface heat flux is gradually weakened (middle orange bars in Fig. 8) and the advective cooling effect by the mean ocean circulation gradually decay with time (not shown), and these two cancel each other out. As a result, the *passive* SST anomaly along the equator is always zonally uniform (Fig. 7b), and the temporal evolution of equatorial Pacific SST warming pattern can be only attributed to the changes in the STC strength.

To further understand the shift in the equatorial Pacific SST warming pattern, two periods with the greatest difference in response patterns are chosen for the following analysis. The first five years (from year 1 to year 5) is taken as the fast response phase (the initial stage), and the last fifty years (from year 101 to year 150) as the slow response phase (the quasi-equilibrium stage). In contrast to the slow response at the quasi-equilibrium stage discussed in Section 3.1, the fast response of SST shows a La Niña-like warming pattern over the equatorial Pacific (i.e., an increased zonal gradient of SST along the equator) (Fig. 10a). At this initial stage, the *passive*

SST anomalies show a widespread warming in the tropics, with a minimum warming at equator and a slight inter-hemispheric asymmetry favoring the northern hemisphere (Fig. 10b); in contrast, the *active* SST anomalies are characterized by a cooling over the tropics, with stronger anomalies in the CEP region and southeast subtropics (Fig. 10c). Similar to what happens during the slow response phase, the east-west gradient of the equatorial Pacific SST during the fast response phase is also dominated by its *active* component. Quantitatively, the zonal SST gradient in the fast response phase is increased by 0.5 °C, which is determined almost entirely by its *active* component (Fig. 10d).

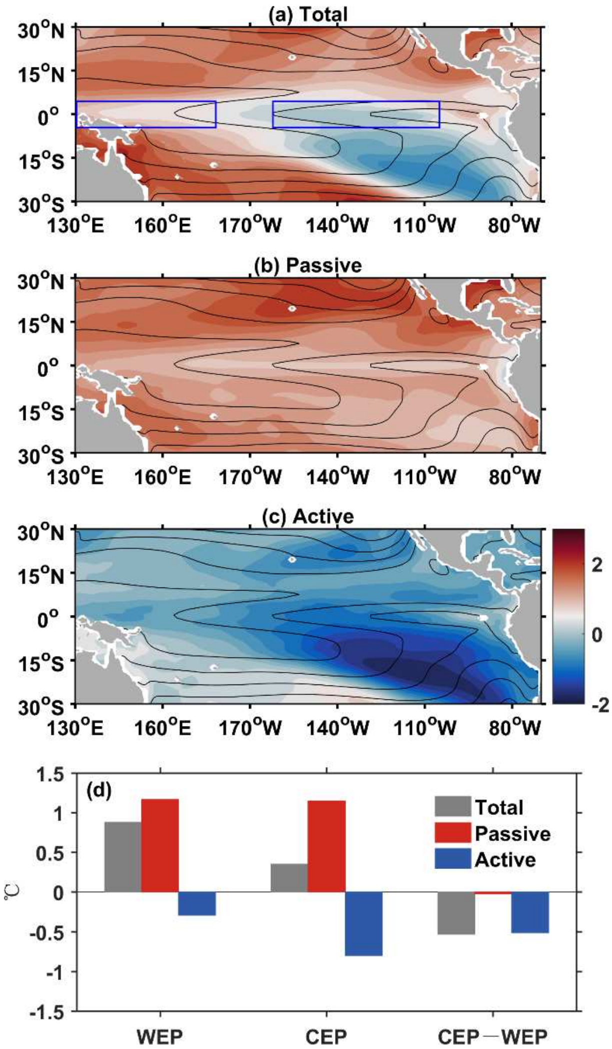

Fig. 10. Same as figure 2 but for the fast response phase.

To help elucidate the processes that maintain the La Niña-like warming pattern during the fast response phase, the mixed layer heat budget analysis is also applied to the initial stage (Fig. 11). Result shows that the warming in the WEP is dominated by changes in the surface heat flux and the residual term, while changes in all ocean heat transport divergence play negative roles (orange bars in Fig. 11a). For the CEP warming, the changes in both the surface heat flux and zonal heat transport divergence have positive contributions, while the changes in the meridional and vertical heat transport divergence contribute negatively (red bars in Fig. 11a). For the increase in the zonal SST gradient (i.e., negative change of CEP−WEP), the main contribution comes from changes in the meridional and vertical heat transport divergence, while the changes in the surface heat flux and zonal heat transport divergence play a damping role (green bars in Fig. 11a). By decomposing the changes in the ocean heat transport divergence into components controlled by ocean circulation change and temperature gradient change, we find that both effects of the meridional and vertical ocean circulation changes (ΔQ_{v2} and ΔQ_{w2}) act to increase the zonal gradient of SST, leading to the La Niña-like warming pattern, which is opposite to their roles in the slow response phase. Specifically, the change in meridional current cools the east more than the west and thus increases the zonal SST gradient along the equator, which can be attributed to the increased southern STC at the initial stage (Fig. 9a) that transports more warm water away from the equatorial eastern Pacific. Meanwhile, the upwelling over the CEP is increased in the fast response phase (not shown), which brings more subsurface cold water up to cool the surface ocean and thus also increase the zonal SST gradient. In addition, the contribution of vertical temperature gradient change (ΔQ_{w1}; the second red bar from the left in Fig. 11e), i.e., the ODT effect, is another effective factor that cools the surface ocean in the CEP region. However, this cooling effect of mean upwelling is balanced with the warming effect of *passive* surface heat flux (middle orange bar in Fig. 8a) in the CEP region, thus the *passive* SST in the fast response phase is also zonally uniform along the equator (Fig. 10b).

In summary, the comparison of the heat budget analyses for the fast and slow response phases shows that the surface heat flux change plays a damping role for the SST pattern formation during both phases, while the ODT effect due to background upwelling cools the CEP region and thus increase the zonal SST gradient in both stages. The major difference between the two stages is the effects of meridional and vertical ocean circulation changes. More specifically, in the fast response phase, the changes of the meridional and vertical ocean circulation (ΔQ_{v2} and ΔQ_{w2}) cool the CEP region, leading to a La Niña-like warming pattern; in the slow response phase, however, their effects become to warm the CEP region, resulting in an El Niño-like warming pattern. This result is consistent with our pervious conclusion that the temporal evolution of the equatorial Pacific SST warming pattern is controlled by the ocean circulation changes, largely via the slowdown of the STCs and the associated changes in the meridional and vertical ocean heat transport divergence.

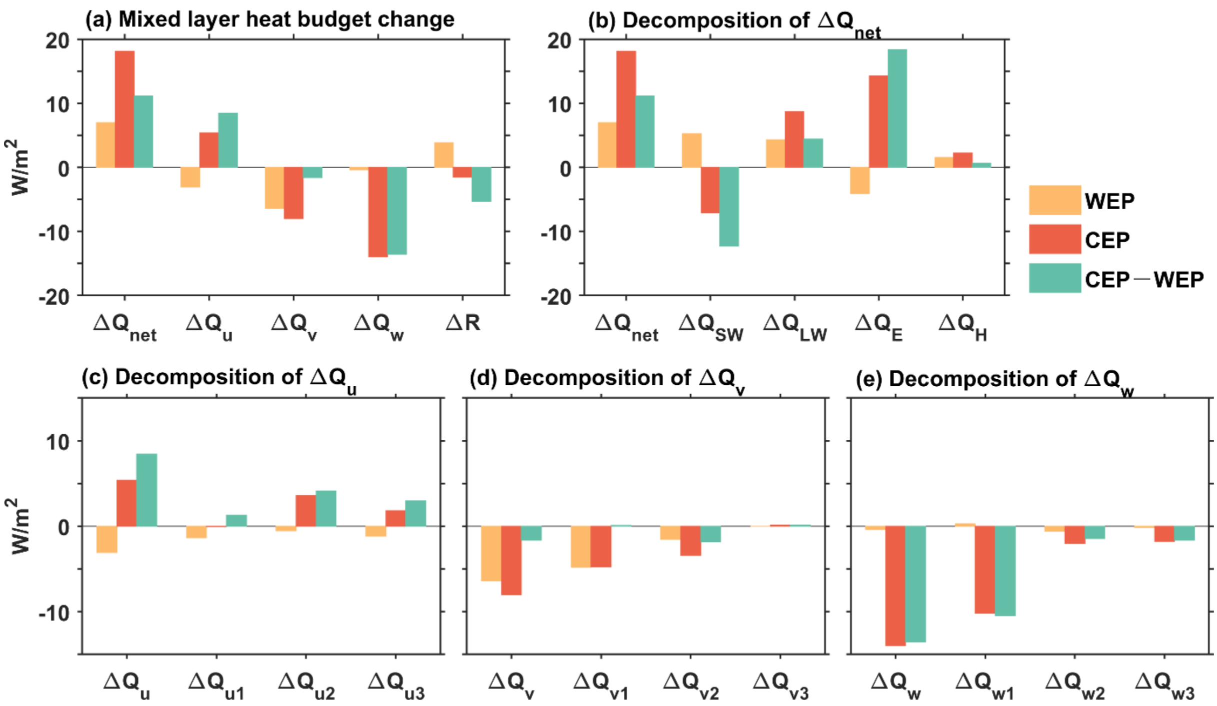

Fig. 11. Same as figure 4 but for the fast response phase.

4 The slab ocean response

It is interesting to compare the warming patterns between the *passive* SST and slab ocean SST response as they are both designed to identify the role of atmospheric processes. The SST response pattern in the slab ocean model bears some resemblance to that in the *passive* component of the PARTIAL (comparing Figs. 12a with 2b), except that there is an El Niño-like warming along the equator in the slab ocean model, corroborating the finding of Vecchi et al. (2008). In addition, the magnitude of the *passive* SST response appears to be weaker than that of the slab ocean model. These differences can be explained by anomalous ocean heat convergence response that is included in the *passive* component but not in the slab ocean model.

In other words, while the effect of the surface flux processes acts on both the *passive* SST and slab ocean SST, the ODT effect only works on the former and balances part of the surface-forced warming in the eastern equatorial Pacific.

It is also worth noting that the *passive* component of tropical SST response is warmer in the northern hemisphere than the southern hemisphere, which is also true in the slab ocean model. This inter-hemispheric asymmetric SST warming pattern may arise from the WES feedback (Xie et al. 2010; Lu and Zhao 2012), consistent with the WES-induced SST pattern in Luo et al. (2015). Figure 12b shows the latent heat flux change due to wind speed change (Q_{EW}) from the slab ocean experiment, which represents the effect of the WES feedback. It can be seen that it matches the SST warming pattern well (Fig. 12). In particular, the weakening of the northeast trade winds leads to stronger SST warming in the northern subtropical Pacific, while the strengthening of the southeast trade winds leads to the minimum warming in the southeast subtropics. This result is consistent with previous studies (Meehl et al. 2007; Lu et al. 2008; Luo et al. 2015). Since the surface flux processes play a similar role in the *passive* SST and the slab ocean SST response, we can infer that the inter-hemispheric asymmetric SST warming pattern of the *passive* component can be mainly attributed to the WES feedback, corroborating the conclusion of Xie et al. (2010) that wind speed change dominates the SST pattern formation in the subtropical Pacific.

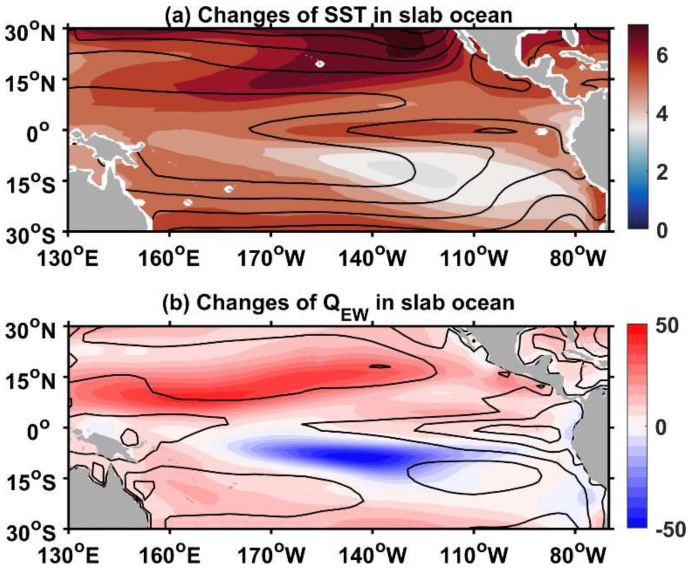

Fig. 12. (a) Changes of SST (°C) in the slab ocean model. Superimposed is mean SST field in CTRL-slab (CI = 2 °C). (b) Changes of latent heat flux due to wind speed change (Q_{EW}; W m^{-2}) in the slab ocean model. Superimposed is mean latent heat flux field in CTRL-slab (CI = 50 W m^{-2}).

5 Conclusion and Discussion

The pattern of equatorial Pacific SST response to global warming is studied in light of a new decomposition of the atmospheric and oceanic processes. To quantify the relative contributions of oceanic and atmospheric processes to the equatorial Pacific SST response to anthropogenic CO_2 forcing, we analyze a pair of fully and partially coupled simulations, the latter being purposefully designed by Garuba et al. (2018a) and Garuba and Rasch (2020). With the assistance of this partially coupled experiment, the SST response due to the surface heat flux and subject to the advection of the mean ocean circulation can be isolated and considered as the atmosphere-forced *passive* component. In contrast, the contribution of the ocean dynamic changes, obtained as the residual of the full temperature response minus the *passive* component, can be considered as the ocean-dynamically induced *active* component.

In response to quadrupled CO_2, the tropical Pacific SST at the slow response or quasi-equilibrium phase is characterized by an El Niño-like warming pattern in the equatorial region and a minimum warming in the southeast subtropics, which are broadly consistent with previous studies (Meehl et al. 2007; Lu et al. 2008; Xie et al. 2010; DiNezio et al. 2013; Kociuba and Power 2015; Luo et al. 2015; Ying et al. 2016; Coats and Karnauskas 2017; Plesca et al. 2018). However, the equatorial Pacific SST warming pattern appears to experience a transition from a fast response to slow response phase. There is an increase of zonal SST gradient along the equator during the fast response phase, followed by a weakening of this SST gradient with time, which conforms with previous studies (Liu 1998; Luo et al. 2017; Heede et al. 2020, 2021). The most important advance in our work is that we can cleanly separate the roles of atmospheric versus ocean dynamic processes in the SST response through a self-consistent decomposition framework.

For the El Niño-like warming pattern at the quasi-equilibrium stage, we find it is entirely determined by the *active* component, while the *passive* SST is characterized by a zonally uniform warming along the equator. The maximum warming in the equatorial eastern Pacific corresponds to the maximum surface heat flux loss, indicating that the surface heat flux plays a damping role in the formation of the El Niño-like warming pattern. Thus, we can conclude that the ocean circulation changes are responsible for the El Niño-like warming pattern by redistributing the background ocean temperature, while the *active* surface heat flux works just to compensate the SST changes. A mixed layer heat budget analysis reveals that the zonal and meridional ocean circulation changes dominate the formation of the El Niño-like warming pattern, and the vertical circulation change plays a positive but secondary role. Specifically, the eastward zonal current anomaly warms the eastern equator by transporting more warm water from the warm pool to the cold tongue, the weakening of the STCs warms the SST in the equatorial eastern Pacific by transporting less warm water away from the equator, and the weakened upwelling over the equatorial eastern Pacific brings slightly less cold waters from the subsurface and thus leads to an increase of SST there. For the air–sea interaction without the ocean dynamical feedbacks, it is found to give rise to a zonally uniform warming along the equatorial Pacific, which is the result of the close balance between the total effect of heat transport divergence associated with mean ocean circulation and the effect of *passive* surface heat flux change. This finding suggests that the effect of ODT in shaping the spatial pattern of the equatorial Pacific SST response to global warming is weaker than previously thought, at least within the model framework used here.

For the temporal evolution of the equatorial Pacific SST response to global warming, we find it is also controlled by the ocean circulation changes. Since the active surface heat flux change over the CEP is negative throughout and thus cannot explain the gradual warming of the active SST in the region over time. In other words, the temporal evolution of the equatorial Pacific SST response is totally dynamically induced. On the basis of previous studies, we conclude that it is the temporal evolution of the STCs, especially its southern branch, that controls the temporal evolution of SST along the equator. Particularly, the change in sign of the zonal SST gradient anomaly coincides with the reversal of changes of the STCs in the southern hemisphere. After 50 years of model integration, as the strength of the STCs stabilizes, so does the zonal gradient of SST along the equator. The role of changes in the STCs on the transition of equatorial Pacific SST warming pattern is further verified with the results of mixed layer heat budget analysis. In particular, the surface heat flux change is found to play a damping role in the formation of both the fast and slow response warming patterns. Meanwhile, the ODT effect cools the CEP region and thus increases the zonal SST gradient in both stages. In the fast response stage, the changes in the meridional and vertical ocean circulations cool the CEP, leading to a La Niña-like warming pattern, while in the slow response stage, they act to warm the CEP, leading to an El Niño-like warming pattern. In summary, the slowdown of the STCs controls the evolution of the equatorial Pacific SST warming pattern by changing the meridional and vertical ocean heat transport divergence. This finding is in contrast to the conclusion from an ocean-only passive tracer experiment in Luo et al. (2017), who found that the decrease of SST zonal gradient with time results largely from the passive advection of warmer extratropical waters by mean STCs. This is due to the fact that their ocean-only passive tracer experiment could not accurately capture the effect of 'passive' surface heat flux change in driving the SST response pattern evolution. Within the atmosphere-ocean coupled framework employed in this study, the *passive* surface heat flux change works together with the mean ocean circulation to drive the temporal evolution of the *passive* SST. The gradually weakening warming effect of the *passive* surface heat flux is accompanied by the gradually declining cooling effect of the mean ocean circulation, and they cancel each other out. As a result, the *passive* SST anomaly along the equator is always zonally uniform, and the temporal evolution of the equatorial Pacific SST warming pattern can only be attributed to the changes of the STCs.

The ocean circulation changes that are fully responsible for the El Niño-like SST warming response to global warming can be driven by changes in both surface winds and buoyancy fluxes. The role of wind-driven ocean circulation change in the equatorial Pacific SST warming has been studied by Luo et al. (2015), who found that the weakening of the equatorial easterlies contributes only 20% to the El Niño-like SST warming pattern. Hence, in combination with Luo et al.'s result, we infer that the ocean circulation change induced by the buoyancy flux change plays a more important role in forming the El Niño-like warming pattern than the wind-driven ocean circulation change. However, the exact role of the buoyancy-induced ocean circulation change on the equatorial Pacific SST response cannot be separated out in either our or Luo et al.'s experimental design. How exactly the buoyancy-induced ocean circulation change contributes to the El Niño-like warming pattern remains an open question for future investigation.

One important caveat of this study is that only one single model with single forcing has been used to decompose the passive and active components. The passive and active decomposition as well as the relative roles of different oceanic and atmospheric processes in the formation of the equatorial Pacific SST warming pattern may vary with different models as the ocean dynamics, cloud feedbacks and other atmospheric mechanisms may differ from model to model. For example, the effect of cloud–shortwave-radiation–SST feedback varies among models, which has been proved as a major source for the model uncertainty in the tropical Pacific SST warming pattern (Ying and Huang 2016). Specifically, the cloud–shortwave-radiation–SST feedback plays a positive role for the weakening of the zonal SST gradient in the ensemble of CMIP5 models, while it plays a negative role in the CESM model. In addition, the ODT effect also behave differently in the models: some models show an increased zonal SST gradient in the initial stage due to strong ODT effect, while others show no ODT effect and thus generate an immediate weakening of the zonal SST gradient in response to CO_2 increase (Heede and Fedorov 2021). Further studies with different models and forcing scenarios will be needed to demonstrate the robustness of the relative importance of the oceanic and atmospheric processes in the formation of the equatorial Pacific SST warming pattern.

Furthermore, it should also be noted that the tropical Pacific response to climate warming might be affected by systematical biases in climate models, such as the tropical Pacific cold tongue bias, overestimation of surface heat flux, underestimation of the Bjerknes feedback, underestimation of local negative SST-cloud feedback, and so on (e.g., Burls et al. 2017; Luo et al. 2018; Seager et al. 2019; Li et al. 2020; Ying 2020; Tang et al. 2021). On the one hand, the projected response of the tropical Pacific may have large model spread due to model biases, so we can expect other models to have different responses than the CESM. For example, different mean state biases in ocean stratification and equatorial upwelling over the tropical Pacific may lead to different ODT effects among models, which further lead to differences in future projections of the tropical Pacific SST (Luo et al. 2018; Heede and Fedorov 2021).

Therefore, future efforts should focus on the relationships between the tropical Pacific response and model biases across different models and how they might affect the uncertainty in future projections. On the other hand, the models' systematic biases may reduce the reliability of the projected changes in the tropical Pacific SST. According to Seager et al. (2022), the CESM tends to bias towards producing a stronger warming trend in the equatorial Pacific than has been observed in recent decades, which may compromise its ability in simulating the response of the tropical Pacific SST to CO_2 forcing. Furthermore, Kohyama and Hartmann (2017) found that most CMIP5 models, including the CESM, cannot reproduce realistic El Niño–Southern Oscillation (ENSO) nonlinearity, which is the reason for their El Niño-like SST response under climate warming. Therefore, further efforts to reduce the common model biases are also needed to help improve projections of climate change in the tropical Pacific.

Notwithstanding the limitations above, by separating the ocean dynamically induced temperature anomaly from the purely atmosphere-forced temperature anomaly, this study directs our attention to the ocean dynamical adjustment as the more likely source for the El Niño-like SST warming pattern in the tropical Pacific under greenhouse gas forcing. In particular, the slowdown of the STCs (especially its southern branch) is found to be the controlling factor for the temporal evolution of the equatorial Pacific SST response to global warming. Thus, the emphasis of the future inquiries into the causal mechanisms for the tropical Pacific SST pattern response should be placed on understanding the ocean dynamical processes and reducing the associated uncertainties.

Acknowledgments

We acknowledge Dr. Oluwayemi Garuba for sharing the data of the fully and partially coupled experiments with tracers. This work is supported by the National Natural Science Foundation of China (NSFC; 42230405 and 41976006) and the Laoshan Laboratory (No. LSKJ202202401). This research used resources of the National Energy Research Scientific Computing Center (NERSC), a U.S. Department of Energy Office of Science User Facility located at Lawrence Berkeley National Laboratory, operated under Contract No. DE-AC02-05CH11231 using NERSC award ERCAP0017151. JL is supported by the U.S. Department of

Energy Office of Science Biological and Environmental Research as part of the Regional and Global Model Analysis program area. Pacific Northwest National Laboratory is operated for DOE by Battelle Memorial Institute under contract DE-AC05-76RL01830.

REFERENCES

An, S.-I., and S.-H. Im, 2014: Blunt ocean dynamical thermostat in response of tropical eastern Pacific SST to global warming. *Theor. Appl. Climatol.*, **118**, 173–183.

Banks, H. T., and J. M. Gregory, 2006: Mechanisms of ocean heat uptake in a coupled climate model and the implications for tracer based predictions of ocean heat uptake. *Geophys. Res. Lett.*, **33**, L07608, https://doi.org/10.1029/2005GL025352.

Bordbar, M. H., T. Martin, M. Latif, and W. Park, 2017: Role of internal variability in recent decadal to multidecadal tropical Pacific climate changes, *Geophys. Res. Lett.,* **44**, 4246–4255

Burls, N. J., L. Muir, E. M. Vincent, and A. Fedorov, 2017: Extra-tropical origin of equatorial Pacific cold bias in climate models with links to cloud albedo. *Clim. Dyn.*, **49**, 2093–2113.

Cai, W., L. Wu, M. Lengaigne, T. Li, S. McGregor, J. S. Kug, et al., 2019: Pantropical climate interactions. *Science*, **363**, eaav4236.

Cane, M. A., A. C. Clement, A. Kaplan, Y. Kushnir, D. Pozdnyakov, R. Seager, S. Zebiak, and R. Murtugudde, 1997: Twentieth century sea surface temperature trends. *Science*, **275**, 957–960.

Clement, A. C., R. Seager, M. A. Cane, and S. E. Zebiak, 1996: An ocean dynamical thermostat. *J. Clim.*, **9**, 2190–2196.

Coats, S., and K. B. Karnauskas, 2017: Are simulated and observed twentieth century tropical Pacific sea surface temperature trends significant relative to internal variability? *Geophys. Res. Lett.*, **44**, 9928–9937.

Collins, M., 2005: El Niño - or La Niña-like climate change? *Clim. Dyn.*, **24**, 89–104.

Collins, M., S-I. An, W. Cai, A. Ganachaud, E. Guilyardi, F-F. Jin, M. Jochum, M. Lengaigne, S. Power, and A. Timmermann, 2010: The impact of global warming on the tropical Pacific Ocean and El Niño. *Nat. Geosci.*, **3**, 391–397.

DiNezio, P. N., A. C. Clement, G. A. Vecchi, B. J. Soden, B. P. Kirtman, and S-K. Lee, 2009: Climate response of the equatorial Pacific to global warming. *J. Clim.*, **22**, 4873–4892.

DiNezio, P. N., B. P. Kirtman, A. C. Clement, S-K. Lee, G. A. Vecchi, and A. Wittenberg, 2012: Mean climate controls on the simulated response of ENSO to increasing greenhouse gases. *J. Clim.*, **25**, 7399–7420.

DiNezio, P. N., G. A. Vecchi, and A. C. Clement, 2013: Detectability of changes in the Walker circulation in response to global warming. *J. Clim.*, **26**, 4038–4048.

England, M. H., S. McGregor, P. Spence, G. A. Meehl, A. Timmermann, W. Cai, A. S. Gupta, M. J. McPhaden, A. Purich, and A. Santoso, 2014: Recent intensification of wind-driven circulation in the Pacific and the ongoing warming hiatus. *Nat. Climate Change*, **4**, 222–227.

Fang, C., and L. Wu, 2008: The role of ocean dynamics in tropical Pacific SST response to warm climate in a fully coupled GCM. *Geophys. Res. Lett.*, **35**, L08703. doi:10.1029/2007GL033097

Fedorov, A. V., and S. G. Philander, 2000: Is El Niño changing? *Science*, **288**, 1997–2002.

Fosu, B., J. He, and G. Liguori, 2020: Equatorial pacific warming attenuated by SST warming patterns in the tropical Atlantic and Indian oceans. *Geophys. Res. Lett.* **47**, e2020GL088231.

Garuba, O. A., J. Lu, F. Liu, and H. A. Singh, 2018a: The active role of the ocean in the temporal evolution of climate sensitivity. *Geophys. Res. Lett.*, **45**, 306–315.

Garuba, O. A., J. Lu, H. A. Singh, F. Liu, and P. Rasch, 2018b: On the Relative Roles of the Atmosphere and Ocean in the Atlantic Multidecadal Variability. *Geophys. Res. Lett.*, **45**, 9186–9196.

Garuba, O. A., and P. J. Rasch, 2020: A partial coupling method to isolate the roles of the atmosphere and ocean in coupled climate simulations. *Journal of Advances in Modeling Earth Systems*, **12**, e2019MS002016. https://doi.org/10.1029/2019MS002016

Gu, D., and S. G. H. Philander, 1997: Interdecadal climate fluctuations that depend on exchanges between the tropics and extratropics. *Science*, **275**, 805–807.

Haney, R. L., 1971: Surface thermal boundary condition for ocean circulation models. *J. Phys. Oceanogr.*, **1**, 241–248.

He, C., A. C. Clement, M. A. Cane, L. N. Murphy, J. M. Klavans, and T. M. Fenske, 2022: A North Atlantic Warming Hole Without Ocean Circulation. *Geophys. Res. Lett.,* **49**, 1–11.

Heede, U. K., A. V. Fedorov, and N. J. Burls, 2020: Time Scales and Mechanisms for the Tropical Pacific Response to Global Warming: A Tug of War between the Ocean Thermostat and Weaker Walker, *J. Clim.*, **33**, 6101-6118.

Heede, U. K., A. V. Fedorov, and N. J. Burls, 2021: A stronger versus weaker Walker: understanding model differences in fast and slow tropical Pacific responses to global warming. *Clim. Dyn.*, **57**, 2505–2522.

Heede, U. K., and A. V. Fedorov, 2021: Eastern equatorial Pacific warming delayed by aerosols and thermostat response to CO_2 increase. *Nat. Clim. Change*, **11**, 696–703.

Held, I. M., and B. J. Soden, 2006: Robust responses of the hydrological cycle to global warming. *J. Clim.*, **19**, 5686–5699.

Hu, S., and A.V. Fedorov, 2017: The extreme El Niño of 2015–2016 and the end of global warming hiatus. *Geophys. Res. Lett.*, **44**, 3816– 3824.

Jin F-F, 1996: Tropical ocean–atmosphere interaction, the Pacific cold tongue, and the El Niño–Southern Oscillation. *Science*, **274**, 76–78.

Kociuba, G., and S. B. Power, 2015: Inability of CMIP5 models to simulate recent strengthening of the Walker circulation: Implications for projections. *J. Clim.*, **28**, 20–35.

Kohyama, T., and D. L. Hartmann, 2017: Nonlinear ENSO Warming Suppression (NEWS). *J. Clim.*, **30**, 4227– 4251.

Kohyama, T., D. L. Hartmann, and D. S. Battisti, 2017: La Niña-like mean-state response to global warming and potential oceanic roles. *J. Clim.*, **30**, 4207–4225.

Kosaka, Y., S.-P. Xie, 2013: Recent global-warming hiatus tied to equatorial Pacific surface cooling. *Nature*, **501**, 403–407.

Kleeman, R., J. P. McCreary Jr., and B. A. Klinger, 1999: A mechanism for generating ENSO decadal variability. *Geophys. Res. Lett.*, **26**, 1743–1746.

Knutson, T. R., and S. Manabe, 1995: Time-mean response over the tropical Pacific to increased CO2 in a coupled ocean– atmosphere model. *J. Clim.*, **8**, 2181–2199.

Li, C., D. Dommenget, and S. McGregor, 2020: Trans-basin Atlantic-Pacific connections further weakened by common model Pacific mean SST biases. *Nat. Commun.*, **11**, 5677.

Li, Q., Y. Luo, J. Lu, and F. Liu, 2022: The Role of Ocean Circulation in Southern Ocean Heat Uptake, Transport and Storage Response to Quadrupled CO_2, *J. Clim.* **35**, 3565-3582.

Liu, F., Y. Luo, J. Lu, and X. Wan, 2017: Response of the tropical Pacific Ocean to El Niño versus global warming. *Clim. Dyn.*, **48**, 935–956.

Liu, Z., 1998: The role of ocean in the response of tropical climatology to global warming: the west–east SST contrast. *J. Clim.*, **11**, 864–875.

Liu, Z., S. J. Vavrus, F. He, N. Wen, and Y. Zhang, 2005: Rethinking tropical ocean response to global warming: the enhanced equatorial warming. *J. Clim.*, **18**, 4684–4700.

Lu, J., and B. Zhao, 2012: The role of oceanic feedback in the climate response to doubling CO_2. *J. Clim.*, **25**, 7544–7563.

Lu, J., G. Chen, and D. Frierson, 2008: Response of the zonal mean atmospheric circulation to El Nino versus global warming. *J. Clim.*, **21**, 5835–5851.

Luo, J. J., G. Wang, and D. Dommenget, 2018: May common model biases reduce CMIP5's ability to simulate the recent Pacific La Niña-like cooling? *Clim. Dyn.*, **50**, 1335-1351.

Luo, Y., J. Lu, F. Liu, and W. Liu, 2015: Understanding the El Niño-like oceanic response in the tropical Pacific to global warming. *Clim. Dyn.*, **45**, 1945–1964.

Luo, Y., J. Lu, F. Liu, and O. Garuba, 2017: The role of ocean dynamical thermostat in delaying the El Niño-like response over the equatorial Pacific to climate warming. *J. Clim.*, **30**, 2811–2827.

Luo, Y., L. M. Rothstein, R.-H. Zhang, and A. J. Busalacchi, 2005: On the connection between South Pacific subtropical spiciness anomalies and decadal equatorial variability in an ocean general circulation model. *J. Geophys. Res.*, **110**, C10002, doi:10.1029/2004JC002655.

Ma, J., and J.-Y. Yu, 2014: Linking centennial surface warming patterns in the equatorial Pacific to the relative strengths of the Walker and Hadley circulations. *J. Atmos. Sci.*, **71**, 3454– 3464.

Ma, S., and T. Zhou, 2016: Robust strengthening and westward shift of the tropical Pacific Walker circulation during 1979– 2012: A comparison of 7 sets of reanalysis data and 26 CMIP5 models. *J. Clim.*, **29**, 3097–3118.

Marshall, J., J. R. Scott, K. C. Armour, J. M. Campin, M. Kelley, and A. Romanou, 2015: The ocean's role in the transient response of climate to abrupt greenhouse gas forcing. *Clim. Dyn.*, **44**, 2287–2299.

McCreary, J. P., Jr., and P. Lu, 1994: Interaction between the subtropical and equatorial ocean circulations: The subtropical cell. *J. Phys. Oceanogr.*, **24**, 466–497.

Meehl, G.A., et al. (2007) Global Climate Projections. In: Climate Change 2007: The Physical Science Basis., *Cambridge University Press*, Cambridge, pp 747–845.

Meng, Q., M. Latif, W. Park, N. S. Keenlyside, V. A. Semenov, and T. Martin, 2012: Twentieth century Walker circulation change: Data analysis and model experiments. *Clim. Dyn.*, **38**, 1757– 1773.

Merlis, T. M., and T. Schneider, 2011: Changes in zonal surface temperature gradients and walker circulations in a wide range of climates. *J. Clim.*, **24**, 4757–4768.

Plesca, E., V. Grützun, and S. A. Buehler, 2018: How robust is the weakening of the Pacific Walker circulation in CMIP5 idealized transient climate simulations? *J. Clim.*, **31**, 81–97.

Rahmstorf, S., and J. Willebrand, 1995: The role of temperature feedback in stabilizing the thermohaline circulation. *J. Phys. Oceanogr.*, **25**, 787–805.

Rivin, I., and E. Tziperman, 1997: Sensitivity of air-sea fluxes to SST perturbations. *J. Clim.*, **10**, 2431–2446.

Ramanathan, V., and W. Collins, 1991: Thermodynamic regulation of ocean warming by cirrus clouds deduced from observations of the 1987 El Niño. *Nature*, **351**, 27–32.

Richter, I., S-P, Xie, 2008: Muted precipitation increase in global warming simulations: a surface evaporation perspective. *J. Geophys. Res.*, **113**, D24118. https://doi.org/10.1029/2008JD010561.

Rodgers, K. B., B. Blanke, G. Madec, O. Aumont, P. Ciais, and J.-C. Dutay, 2003: Extratropical sources of equatorial Pacific upwelling in an OGCM. *Geophys. Res. Lett.*, **30**, 1084, https://doi.org/10.1029/2002GL016003.

Schneider, E. K., M. J. Fennessy, and J. L. Kinter, 2009: A statistical–dynamical estimate of winter ENSO teleconnections in a future climate. *Clim. Dyn.*, **22**, 6624–6638.

Seager, R., and R. Murtugudde, 1997: Ocean dynamics, thermocline adjustment and regulation of tropical SST. *J. Clim.*, **10**, 521–534.

Seager, R., M. Cane, N. Henderson, D.-E. Lee, R. Abernathey, and H. Zhang, 2019: Strengthening tropical Pacific zonal sea surface temperature gradient consistent with rising greenhouse gases. *Nat. Clim. Change*, **9**, 517–522.

Seager, R., N. Henderson, and M. Cane, 2022: Persistent Discrepancies between Observed and Modeled Trends in the Tropical Pacific Ocean, *J. Clim*., **35**, 4571-4584.

Tang, T., J. J. Luo, K. Peng, L. Qi, and S. Tang, 2021: Over-projected Pacific warming and extreme El Niño frequency due to CMIP5 common biases, *Natl. Sci. Rev.*, **8**, nwab056, https://doi.org/10.1093/nsr/nwab056.

Vecchi, G. A., B. J. Soden, A. T. Wittenberg, I. M. Held, A. Leetmaa, and M. J. Harrison, 2006: Weakening of tropical Pacific atmospheric circulation due to anthropogenic forcing. *Nature*, **441**, 73–76.

Vecchi, G. A., B. J. Soden, 2007: Global warming and the weakening of the tropical circulation. J. Clim., 20, 4316–4340.

Vecchi, G. A., A. C. Clement, and B. J. Soden, 2008: Examining the tropical Pacific's response to global warming. *Eos, Trans. Amer. Geophys. Union*, **89**, 81–83.

Wang, C., 2006: An overlooked feature of tropical climate: Inter-Pacific-Atlantic variability. *Geophys. Res. Lett.* **33**, L12702.

Wang, C., 2019: Three-ocean interactions and climate variability: a review and perspective. *Clim. Dyn.* **53**, 5119–5136.

Xie, S.-P., C. Deser, G. A. Vecchi, J. Ma, H. Teng, and A. T. Wittenberg, 2010: Global warming pattern formation: sea surface temperature and rainfall. *J. Clim.*, **23**, 966–986.

Xie, P., and G. K. Vallis, 2012: The passive and active nature of ocean heat uptake in idealized climate change experiments. *Clim. Dyn.*, **38**, 667–684.

Yamanaka, G., H. Tsujino, H. Nakano, and M. Hirabara, 2015: Decadal variability of the Pacific subtropical cells and its relevance to the sea surface height in the western tropical Pacific during recent decades. *J. Geophys. Res. Oceans*, **120**, 201–224.

Ying, J., P. Huang, and R. Huang, 2016: Evaluating the formation mechanisms of the equatorial Pacific SST warming pattern in CMIP5 models. *Adv. Atmos. Sci.*, **33**, 433–441.

Ying, J., and P. Huang, 2016: Cloud–Radiation Feedback as a Leading Source of Uncertainty in the Tropical Pacific SST Warming Pattern in CMIP5 Models, *J. Clim.*, **29**, 3867-3881.

Ying, J., 2020: Sources of Uncertainty in the Tropical Pacific Warming Pattern under Global Warming Projected by Coupled Ocean-Atmosphere Models, *Springer Theses,* https://doi.org/10.1007/978-981-32-9844-6_7

Ying, J., M. Collins, W. Cai, A. Timmermann, P. Huang, D. Chen, K. Stein, 2022: Emergence of climate change in the tropical Pacific. *Nat. Clim. Change*, **12**, 356–364.

Zhang, L., W. Han, K. B. Karnauskas, G. A. Meehl, A. Hu, N. Rosenbloom, and T. Shinoda, 2019: Indian Ocean warming trend reduces Pacific warming response to anthropogenic greenhouse gases: An interbasin thermostat mechanism. *Geophys. Res. Lett.*, 46, 10882–10890.

Statements and Declarations

Funding: This work is supported by the National Natural Science Foundation of China (NSFC; 42230405 and 41976006) and the Laoshan Laboratory (No. LSKJ202202401). This research used resources of the National Energy Research Scientific Computing Center (NERSC), a U.S. Department of Energy Office of Science User Facility located at Lawrence Berkeley National

Laboratory, operated under Contract No. DE-AC02-05CH11231 using NERSC award ERCAP0017151. JL is supported by the U.S. Department of Energy Office of Science Biological and Environmental Research as part of the Regional and Global Model Analysis program area. Pacific Northwest National Laboratory is operated for DOE by Battelle Memorial Institute under contract DE-AC05-76RL01830.

Competing interests: The authors have no relevant financial or non-financial interests to disclose.

Author contributions: Y. Luo, J. Lu and F. Liu were responsible for design of the research. The first draft of the manuscript was written by Q. Li and all authors commented on previous versions of the manuscript. All authors read and approved the final manuscript.

Data Availability: The CESM data used in this study are available from the corresponding author upon request.